Investigation of Dynamic and Static Recrystallization Behavior During Thermomechanical Processing in a API-X70 Microalloyed Steel

Bahman Mirzakhani, Mohammad Taghi Salehi, Shahin Khoddam, Seyed Hosein Seyedein, and Mohammad Reza Aboutalebi

Recovery and recrystallization phenomena and effects of microalloying elements on these phenomena are of great importance in designing thermomechanical processes of microalloyed steels. Control of these phenomena can lead to manufacturing of products with suitable structures and desirable properties. The aim of this study was to investigate the microstructural evolution occurring during thermomechanical processing through hot compression testing. The niobium carbonitride approximate solution temperature was initially determined to guess the optimum reheating temperature. Then continuous and interrupted compression tests were utilized to physically model the dynamic and static recrystallization (SRX) behavior of the steel during thermomechanical processing. The parameters of the flow stress model and the activation energy of dynamic recrystallization (DRX) were calculated and the effects of deformation conditions on peak strain of DRX were evaluated. In addition, a kinetic study of the static softening of austenite indicated that the plateau occurred in recrystallization fraction-time curves below 1025 °C. This was considered in determining the Static Recrystallization Critical Temperature (SRCT) and construction of the Recrystallization Retardation-Temperature Time (RRTT) diagram for this steel.

1. Introduction

Thermomechanical processing has been extensively used by industries in the past decades. The ultimate goal of these efforts is to achieve desired properties such as high strength, ductility, or toughness (Ref 1, 2).

The mechanical properties of materials are usually influenced by their microstructures. Thus, understanding and modeling of microstructure evolution during hot deformation, and the effect of thermomechanical parameters on the flow stress of a material, is critical for optimizing processing conditions in order to improve product properties.

As steel is deformed, the internal energy increases through the storage of dislocations. During hot deformation of steels various softening processes occur to reduce the internal energy of the deformed metal. In alloys having low stacking fault energy such as the austenite phase in steel, the rate of dislocation annihilation due to the recovery mechanism is not enough to compete with the strain hardening rate, so the dislocation density increases continuously. When the internal energy reaches a threshold value, the deformed grains may be replaced by new strain-free grains via the recrystallization mechanism (Ref 3). When recrystallization occurs concurrently with deformation, the process is called dynamic recrystallization (DRX) and when it occurs after deformation, it is termed static recrystallization (SRX). In some cases DRX may initiate through nucleation, but may not proceed to completion during deformation. In these cases, the recrystallization is completed after deformation by the growth of dynamically nucleated grains. This is known as Metadynamic or post dynamic recrystallization (MDRX). The conditions under which SRX, DRX, and MDRX occur are determined by the combination of processing parameters.

In addition to strain hardening, precipitation of microalloying elements in steels may harden the austenite during hot deformation and precipitation may retard the subsequent softening. This retarding effect of microalloying elements has been shown in many studies (Ref 4-11). In recent years, physical modeling of microstructure evolution during thermomechanical process by hot torsion, hot compression, and hot tension has become a powerful tool to investigate the softening behavior of various alloys during hot deformation processes (Ref 4-9 and 11-15).

The aim of the present research was physical modeling of the softening behavior of the austenite in API-X70 microalloyed steel, of gas and oil line pipe, by using hot compression testing. The evolution of the initial austenite grains in the reheating treatment was studied as well. This will help to improve understanding of the microstructure evolution during various stages of thermomechanical processing, used for producing this steel.

Bahman Mirzakhani, Mohammad Taghi Salehi, Seyed Hosein Seyedein, and **Mohammad Reza Aboutalebi**, Department of Metallurgical Engineering, Iran University of Science and Technology, P.O. Box 16844-13114, Tehran, Iran; and **Shahin Khoddam**, Department of Mechanical Engineering, Monash University, Clayton Campus, Melbourne, Victoria 3800, Australia. Contact e-mails: bmirzakhani@iust.ac.ir, salehi@iust.ac.ir, shahin.khoddam@eng.monash.edu.au, seyedein@iust.ac.ir and mrezab@iust.ac.ir.

2. Materials and Experimental Procedure

The chemical composition of the Nb-V microalloyed steel used in this study is given in Table 1. This composition was designed for new line pipe material. Several bars of this steel were casted by melting the raw materials and alloying the elements in a laboratory atmosphere controlled induction furnace supplied with an argon gas. The ingots were homogenized at 1300 °C for 30 min and hot rolled in five passes at temperature ranges of 1000-1200 °C to remove the casting microstructure. The final thickness of the plates produced was approximately 20 mm. For hot compression tests, cylindrical specimens with 15 mm height and initial diameters of 10 mm were cut out from these plates. The cylindrical axis was perpendicular to rolling direction and parallel to the thickness of the plates.

For determining the optimum reheating temperature before hot deformation, seven samples were austenitized at 1300, 1275, 1250, 1225, 1200, 1150, and 1100 °C for 15 min and then quenched in water. For optical microscopic examination, the initial austenite grain boundaries were revealed by etching the samples in either 2% Nital or warm supersaturated solution of picric acid. The austenite grain size was calculated with the lineal intercept (or Heyn) metallographic procedure according to ASTM E1121 (Ref 16) and the effect of reheating temperature on initial austenite grain size was studied.

The specimens were reheated in an argon atmosphere controlled furnace with 5 °C/s to 1275 °C, held for 15 min and cooled with 10 °C/s to the prescribed deformation temperature, and then held for 1 min at this temperature before being subjected to hot compression. These tests were carried out in an INSTRON8500 machine. This machine had a maximum load of 20,000 kg, a maximum available rate of 0.1 s^{-1} and was equipped with a resistance heating system. Graphite was used as a lubricant and mica foil was used to prevent carbon diffusion into the specimen at high reheating temperatures. The load, displacement, and temperature were recorded in a digital system. The flow curves of true stress versus true strain were then plotted for various test conditions. Continuous and interrupted hot compression experiments preprogrammed according to Table 2.

Table 1 Chemical composition of the Nb-V microalloyed steel (wt.%)

C	Mn	Si	P	S	Nb	V	N	Fe
0.142	1.44	0.34	0.013	0.009	0.044	0.095	0.009	Rem.

Table 2 Hot deformation conditions of present study

Thermomechanical parameter	Hot compression test	
	Continuous	**Interrupted**
Reheating temperature, °C	1275	1275
Deformation temperature, °C	1150, 1100, 1050	1050, 1025, 1000, 975, 950
True strain	0.8	0.15
True strain rate, s^{-1}	0.01, 0.05, 0.1	0.1
Interpass time, s	···	30, 60, 100, 150, 300

In the continuous deformation experiments, the effects of temperatures and strain rates on the strength of the austenite were investigated. Also, in interrupted hot compression tests, the kinetics of static softening were investigated in order to study the effects of microalloying elements on recrystallization retardation and flow stress of the steel during thermomechanical processing.

3. Results and Discussion

3.1 Reheating Treatment

The effect of the reheating temperature prior to deformation on austenite grain size is illustrated in Fig. 1. This figure shows that, in the temperature range of 1100-1240 °C, austenite grain growth was slow with a normal trend, but at higher temperatures than 1240 °C it became rapid. The progress of grain growth with increasing reheating temperature is illustrated in this figure. At 1300 °C the mean grain size of the austenite was 558 μm, which in comparison with the size of grain at 1100 °C (i.e., 68 μm), shows 720% grain growth. It is said (Ref 17) that the grain boundary migration is a function of particle precipitations within the grain boundaries. The higher the number of these particles, the lower will be the boundary migration. According to Eq 1 (Ref 18), the solution temperature of the Nb precipitates is about 1250 °C:

$$\log\left\{[\text{Nb}] \cdot \left[C + \frac{12}{14}N\right]\right\} = 2.26 - \frac{6770}{T} \qquad \text{(Eq 1)}$$

where C, Nb, N, respectively, are contents of carbon, niobium, and nitrogen (wt.%) in steel and T is dissolution temperature of Nb(C,N) in Kelvin. So at temperatures higher than 1240 °C, it seemed some of the Nb precipitates present at grain boundaries, were dissolved. Therefore, an easier condition for the boundary migration seemed to be provided. It is logical to expect the pinning effect of grain boundary particles at higher temperatures than 1240 °C to be less effective in preventing the grain growth.

It should be noted that vanadium carbide, nitride, and carbonitride particles dissolve within the range of 850-984 °C according to Andrade et al. (Ref 5). On the other hand, reheating the samples in a temperature range of 1100-1300 °C
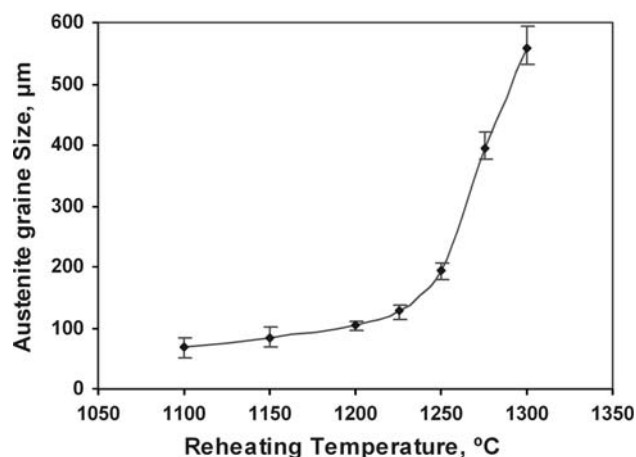

Fig. 1 Variation of austenite grain size with reheating temperature

led to complete dissolution of vanadium precipitates. So one can assume the small amount of grain growth at lower temperatures than 1240 °C was due to preventing effects of Nb(C, N) particles, which were still stable at this temperature. However, at higher temperatures, i.e., above 1250 °C, which is the dissolution temperature of Nb(C, N) precipitates, it seems these particles were dissolved and this resulted in enormous grain growth.

On the base of this observation, a higher reheating temperature of 1275 °C, before subjecting the samples to hot compression, was chosen. This reheating temperature was chosen to shorten the dissolution time of the microalloying precipitates, in order to ensure all the microalloying particles dissolved before deformation. This was done to investigate the effects of these elements on subsequent softening phenomena. The initial austenite grain size of the steel prior to hot deformation was 395 μm.

3.2 Dynamic Recrystallization

Figure 2 shows the flow curves obtained for various deformation conditions. At all temperatures and strain rates (except at 1050 °C and 0.1 s^{-1}), the curves display a rapid initial raise to maximum points, characterized by the peak stress σ_P and strain ε_P, followed by a gradual fall to a steady state stress σ_{SS}. This trend indicates the occurrence of the DRX process.

Figure 2 indicates that when the temperature decreases or when the strain rate increases, σ_P and ε_P increase. This caused the initiation of DRX process to occur at larger strains.

The effect of the deformation conditions on the critical strain (ε_C) of the DRX process was further confirmed by the following equations:

$$\varepsilon_C = a\varepsilon_P \qquad (Eq\ 2)$$

$$\varepsilon_P = kD_o^p Z^q \qquad (Eq\ 3)$$

$$Z = A(Sin\,h\,\alpha\,\sigma_P)^{n'} = \dot{\varepsilon}\exp\left(\frac{Q_{def}}{RT}\right) \qquad (Eq\ 4)$$

where a, k, p, q, A, α, and n′ are constants, D_o is the initial austenite grain size, Z is the Zener-Hollmon parameter, Q_{def} is the activation energy of deformation, R is the universal gas constant, and T is the absolute temperature. These equations indicate that as Z increases (at higher strain rate and lower temperature), the work hardening rate increases, which in turn leads to an increase in σ_P and ε_C.

For the construction of a flow stress model and calculation of Q_{def}, the relation between $\log\dot{\varepsilon}$ and $\log(Sin\,h\,\alpha\,\sigma_P)$, and $\log(Sin\,h\,\alpha\,\sigma_P)$ and 1000/T were examined in Fig. 3. The values of $\alpha = 0.05$ and n′=1.645 were obtained from Eq 4. The slope of $\log(Sin\,h\,\alpha\,\sigma_P) - 1000/T$ lines (S) from Fig. 2(b) is equal to:

$$\frac{Q_{def}}{2.3n'RT} = Slope \qquad (Eq\ 5)$$

The calculated value of Q_{def} was 284 KJmol^{-1} for DRX process. This is within the range of observations of other studies such as Reference 12 and 13.

Comparing values of ε_P, σ_P, and σ_{SS} in the present study with the values of these parameters reported (Ref 15) for a C-Mn steel having the same content of carbon and manganese and deformed under the same conditions (the same Z value), indicates that the presence of solute Nb in the steel under study
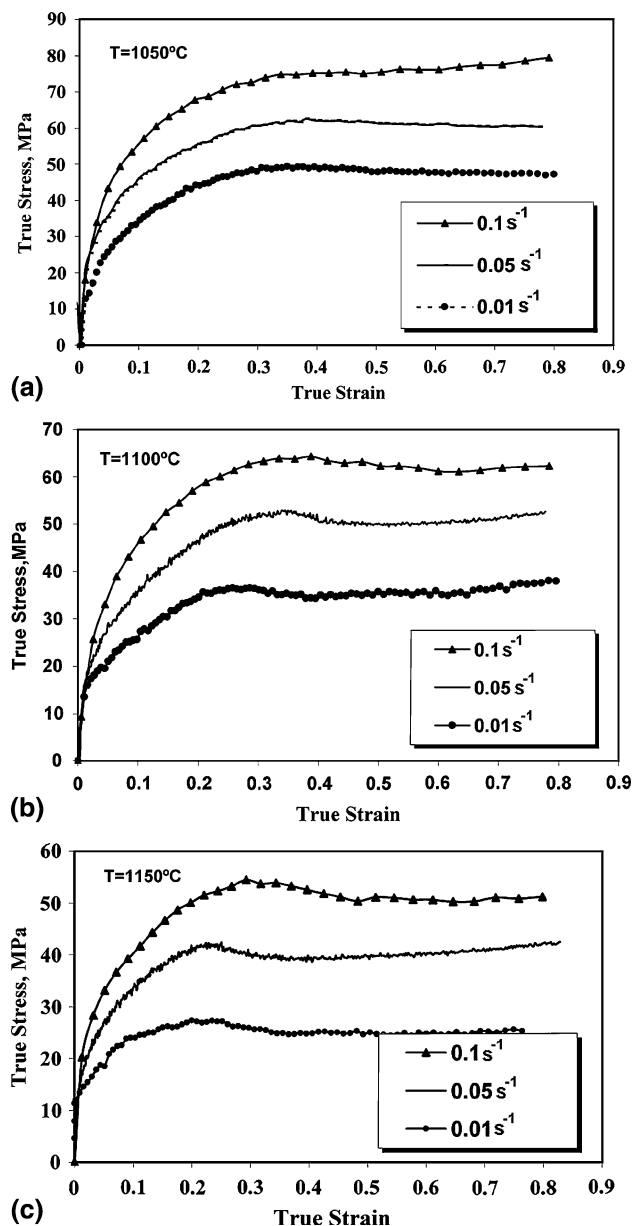

Fig. 2 Flow curves of the samples deformed at strain rates of 0.01, 0.05, and 0.1 s^{-1}, and temperature of (a) 1050 °C, (b) 1100 °C, and (c) 1150 °C

caused a rise in the peak and steady stresses between 5 and 10 MPa. It also caused a 0.15 increase in the critical strain for onset of DRX. This rise is an indication of softening retardation. It has been reported that precipitation strengthening of Nb occurs at a temperature of 950 °C or below (Ref 5, 11, and 19). Therefore it is expected that cooling the samples from the reheating temperature to the prescribed deformation temperature (i.e., 1150, 1100, 1050 °C), using a fairly high cooling rate, could not lead to formation of Nb precipitates. In other words, the entire amount of V in bulk (0.095 wt.%) and nearly the entire amount of Nb remain still in solution before starting deformation. It has also mentioned (Ref 5) that the solute drag effect of Nb is much stronger than that of V. As dynamic precipitation of Nb rich particles occurs below 900 °C and at very low strain rates according to Ref 19, it can be deduced that the retardation of the onset of DRX and the increase of peak
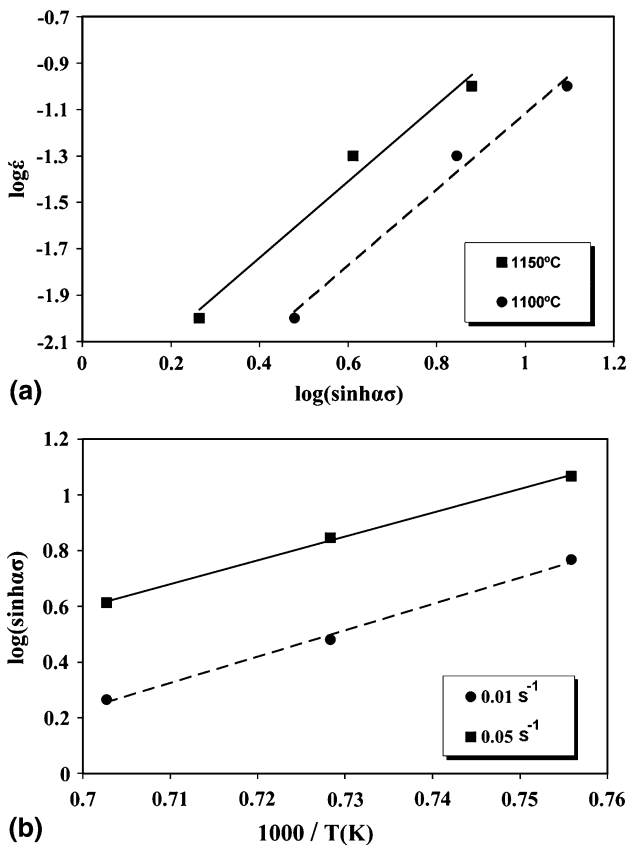
Fig. 3 Variation of (a) $\log \dot{\varepsilon}$ versus $\log(\mathrm{Sin\,h\,\alpha\,\sigma_P})$ at 1150 and 1100 °C, (b) $\log(\mathrm{Sin\,h\,\alpha\,\sigma_P})$ versus $1000/T$ at 0.05 and 0.01 s^{-1}
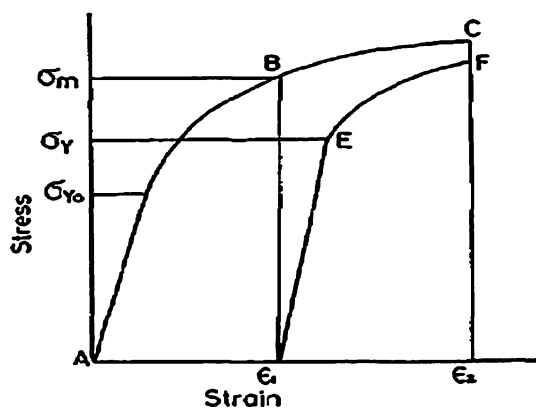

Fig. 4 Schematic representation of stress-strain curves in intermittent double-stage hot compression

and steady stresses within the present steel related to solute drags of Nb atoms. The Nb atoms or its clustering can halt the annihilation or re-arrangement of dislocations introduced during deformation.

3.3 Static Recrystallization

Interrupted or double-stage hot compression tests were conducted to monitor the SRX kinetics. The stress-strain curves for the first and the second stages of the interrupted hot compression test are shown schematically in Fig. 4. In this test after the first stage of deformation, material is work-hardened
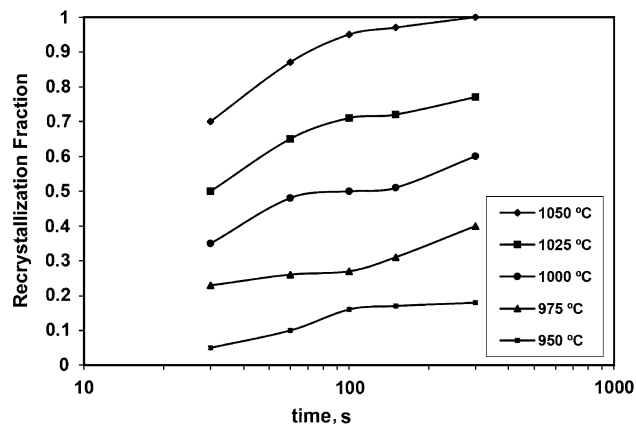

Fig. 5 Kinetic of static recrystallization at a constants strain of 0.15 and strain rate of 0.1 s^{-1}

and the yield stress σ_{Y0} increases to σ_m. While the sample is held for a selected time, and keeping the deformation temperature constant, the compressive stress is relaxed. Then the sample is deformed again under the same temperature, strain, and strain rate conditions used in the first stage. In the second hit the yield stress of the material becomes σ_Y. A constant true strain of 0.15, true strain rate of 0.1 s^{-1} and temperatures of 1050, 1025, 1000, 975 and, 950 °C were used in the present research. The interpass time was varied from 30 s to 300 s.

Using the 2% yield stress the recrystallized fraction (X_{SRX}) after an interrupted hot working was calculated from the following expression:

$$X_{SRX} = \frac{\sigma_m - \sigma_Y}{\sigma_m - \sigma_{Y0}} \qquad (Eq\ 6)$$

where σ_m is the applied flow stress for work-hardened steel, σ_{Y0} is the flow stress at yield point for a fully recrystallized specimen, and σ_Y is the flow stress of a partially recrystallized specimen. Indeed the effect of solutes and precipitates in Eq 6 is incorporated indirectly through the stress levels. The solute drags and precipitates delay the softening and lead to an increase of flow stresses in the material in the first or/ and the second stages of deformation. For example if the precipitation happens during interpass time, it may cause an increase of σ_Y, which in turn decreases the amount of fraction of recrystallization. It is worth noting that Fernandez et al. (Ref 14) reported that using the 2% offset method excludes recovery effects better, and describes more suitably the SRX kinetics of microalloyed steels.

The effect of the deformation temperature and intermittent time on the SRX fraction is presented in Fig. 5. This figure shows that by increasing the compression temperature, the softening kinetics of the specimen were accelerated so that at temperatures higher than 1025 °C, the recrystallization fraction exceeded 50% even at short interpass times. This is an indication of a decrease in dislocation density. In other words, the prominent increase in austenite strength during controlled rolling practice seems primarily caused by strain accumulation, due to the development of a non-recrystallized austenitic structure.

Figure 5 also shows, at temperatures lower than or equal to 1025 °C, that the recrystallization fraction remains constant in a given time range for each temperature. This is the plateau part of
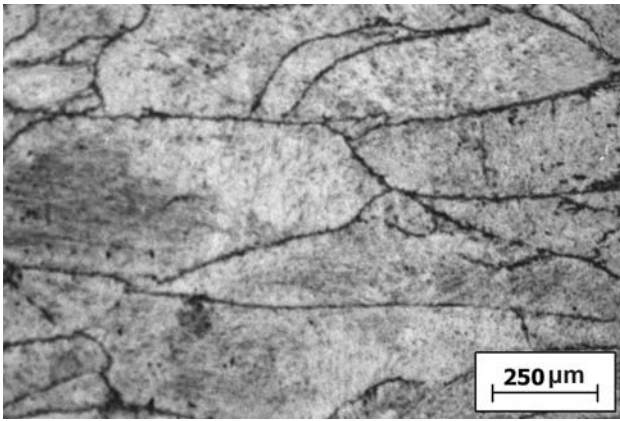
Fig. 6 Austenitic microstructure of specimen deformed at 950 °C, true strain of 0.15 at true strain rate of 0.1 s^{-1} and holding time 300 s

Fig. 7 Recrystallization retardation time as a function of temperature (RRTT diagram) at a constants strain of 0.15 and strain rate of 0.1 s^{-1}

each curve shown in this figure. This part usually occurs in all microalloyed steels according to Reference [6-8], [10], [20], and [21] and gives rise to a strain accumulation and an increase in the internal energy. The plateau section within the softening curves indicates the progress of strain induced precipitation, such as Nb(C, N) formation, which possibly delayed further recrystallization. This is due to the fact that the preferential nucleation sites for both recrystallization and precipitation are known to be the same: prior austenite grain boundaries and dislocation substructures. The microstructure of the sample deformed at 950 °C, and held at this temperature for a long time, i.e., 300 s, is presented in Fig. 6. The elongated austenite grains in this figure illustrate that no recrystallization occurred in this sample. However, according to Fig. 5 softening fraction of the sample was 0.2. It has been reported that up to about 12% of the fractional softening is associated with the static recovery process (Ref [5]). Therefore, some part of the softening fraction of this sample might be related to softening via the recovery process.

The plateau section for various temperatures started at different times, as indicated above, however the softening curve of the compression test performed at 1050 °C did not show this section. The apparent plateau in 1050 °C in Fig. 5 seems not to relate to the strain induced precipitations, because there is a decline in driving force in the end of recrystallization. This gives a typical sigmoid shape to the kinetics' curve. This means that at this temperature or higher temperatures, precipitation did not occur after deformation during holding interpass time. The temperature below which the plateau starts to appear in this study was 1025 °C. This temperature is known as the Static Recrystallization Critical Temperature (SRCT), which was lower than the solubility temperature, as reported by Medina et al. (Ref [6]). This is to say that at a lower temperature than SRCT, strain induced precipitation started, and the occurrence of this phenomenon depended on chemical composition and all other hot deformation conditions. Recrystallization restarted at the end of the plateau, so that the recrystallization fraction, X_{SRX}, continuously increased as shown in Fig. 5.

The extents of the plateau sections presented in Fig. 5 were determined, in order to construct the Recrystallization Retardation-Temperature Time (RRTT) diagram. The result was drawn in Fig. 7. This figure shows that at 975 °C, the precipitates had a high suppression effect on the softening phenomena which corresponded to the nose of the P_S curve. In
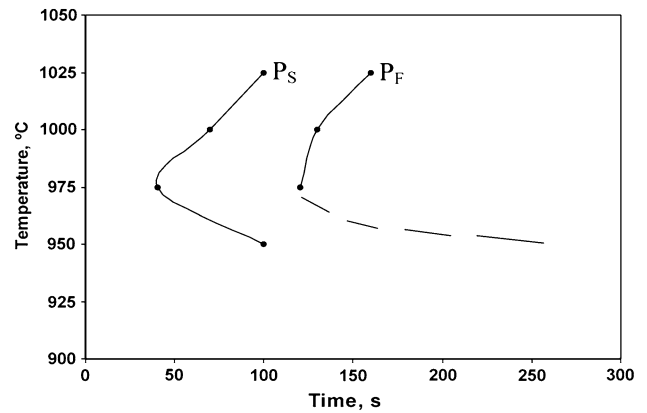
other words, at this temperature the incubation time for precipitation was the least, so that the volume fraction of the precipitates within the microstructure was high enough to have a maximum influence on halting the annihilation of dislocations. However, the effect of precipitates on the suppression of recrystallization started at later times, at both higher and lower temperatures than 975 °C. This is due to either an insufficient volume fraction of precipitates, or loosing the pinning effect of coarse precipitates on dislocation movements. As mentioned earlier, effective suppression of recrystallization is possible by a small volume fraction of precipitates. At higher temperatures an insufficient driving force for precipitate nucleation and at lower temperatures a diminishing diffusion rate for promoting precipitation formation caused the volume fraction of precipitates not to be high enough to halt recrystallization in short intermittent times. Additionally, dislocation annihilation occurring during the recrystallization process decreases the number of preferential nucleation sites for precipitates, when recrystallization starts before precipitation.

It has been reported (Ref [5] and [8]) that vanadium induced precipitation occurs at temperature below 900 °C. So at a temperature range 950-1050 °C this element appeared to exist in the form of solution. Therefore the microalloying element that affected the retardation of recrystallization in this study seemed to be niobium.

Kown and DeArdo (Ref [4]) reported that the pinning force of precipitates increases as the precipitation of the particles progresses, and after a while it decreases due to precipitation coarsening. According to this point of view, the end point of plateau in each softening curve observed in this study (P_F curve in Fig. 7) shows that precipitates started to coarsen and loose their effect on recrystallization retardation. Meanwhile, when the temperature increased, precipitation coarsening was so fast that the plateau of SRX curves became shorter.

It is predicted that each parameter which promotes precipitation formation and coarsening, shifts the P_S and the P_F curves to the right in Fig. 7. Increasing the strain, strain rate, and decreasing the reheating treatment may lead to this shift. In other words, a higher dislocation density results in a higher nucleation rate and precipitate fraction, and this supports much impact on retardation of softening. Meanwhile, it is known that diffusion through dislocations provides precipitate coarsening rapidly in comparison to low dislocation density.

Knowing the SRCT of microalloyed steels is of great importance in thermomechanical controlled rolling processing (TMCP). One can say the final passes in a rolling process which take place at temperatures below SRCT will give rise to an accumulated strain in the austenite. Hence a small ferrite grain size can be attained from heavily deformed austenite if the successive passes are carried out at temperatures above SRCT.

Recrystallization Retardation-Temperature Time diagrams can help to find out in which temperature of finishing passes in plate mills partial recrystallization may take place. Partial recrystallization leading to mixed grain sizes is impractical from the point of view of thermomechanical processing (Ref 1-3).

4. Conclusions

1. A plot of austenite grain size versus reheating temperature provides an effective practical method for determining the solution temperature of microalloying precipitates.
2. Increasing the strain rate and/or decreasing the compression temperature caused a raise in the critical strain of DRX in this study.
3. The Nb-V microalloyed steel presented a higher value of critical strain for starting DRX, in comparison with that of plain carbon steel at identical Z, which is related to Nb atom solute drag effect.
4. At temperatures lower than or equal to 1025 °C, the plateau occurred in kinetic curves of SRX.
5. The plateau of SRX curves became shorter as the compression temperature increased.

Acknowledgment

References

1. P.D. Hodgson and M.R. Barnett, The Thermomechanical Processing of Steels Current and Future Trends, Metal Forming 2000, *Proceedings of the 8th International Conference on Metal Forming*, M. Pietrzyk et al., Eds., (Rotterdam), Balkema, 2000, p 21–28
2. C. Ouchi, Development of Steel Plates by Intensive Use of TMCP and Direct Quenching Processes, *ISIJ Int.*, 2001, **41**(6), p 542–553 (in English)
3. F.J. Humphreys and M. Hatherly, *Recrystallization and Related Annealing Phenomena*, 2nd ed., Pergamon, Oxford, 2004
4. O. Kwon and A.J. DeArdo, Interactions Between Recrystallization and Precipitation in Hot-Deformed Microalloyed Steels, *Acta Metall. Mater.*, 1991, **39**(4), p 529–538 (in English)
5. H.L. Andrade, M.G. Akben, and J.J. Jonas, Effect of Molybdenum, Niobium, and Vanadium on Static Recovery and Recrystallization and Solute Strengthening in Microalloyed Steels, *Metall. Trans.*, 1983, **14A**, p 1967–1977 (in English)
6. S.F. Medina and J.E. Mancilla, Static Steels Recrystallization at Temperatures Modeling Below of the Hot Deformed Microalloyed Critical Temperature, *ISIJ Int.*, 1996, **36**(8), p 1070–1083 (in English)
7. S.F. Medina and J.E. Mancilla, Determination of Static Recrystallization Critical Temperature of Austenite in Microalloyed Steels, *ISIJ Int.*, 1993, **33**(12), p 1257–1264 (in English)
8. S.F. Medina and A. Quispe, Improved Model for Static Recrystallization Kinetics of Hot Deformed Austenite in Low Alloy and Nb/V Microalloyed Steels, *ISIJ Int.*, 2001, **41**(7), p 774–781 (in English)
9. R. Abad, A.I. Fernandez, B. Lopez, and J.M. Rodriguez, Interaction Between Recrystallization and Precipitation During Multipass Rolling in a Low Carbon Niobium Microalloyed Steel, *ISIJ Int.*, 2001, **41**(7), p 1373–1382 (in English)
10. K.J. Lee, Recrystallization and Precipitation Interaction in Nb Containing Steels, *Scr. Mater.*, 1999, **40**(7), p 837–843 (in English)
11. J. Perttula, P. Kantanen, and P. Karjalainen, Effect of Precipitation on Flow Stress and Recrystallization in Nb- and Ti-Bearing Austenite, *Scand. J. Metall.*, 1998, **27**, p 128–132 (in English)
12. S.H. Cho, K.B. Kang, and J. Jonas, The Dynamic, Static and Metadynamic Recrystallization of a Nb-Microalloyed Steel, *ISIJ Int.*, 2001, **41**(1), p 63–69 (in English)
13. M. Carsi, V. Lopez, F. Penalba, and O.A. Ruano, The Strain Rate as a Factor Influencing the Hot Forming Simulation of Medium Carbon Microalloyed Steels, *Mater. Sci. Eng.*, 1996, **216A**, p 155–160 (in English)
14. A.I. Fernandez, B. Lopez, and J.M. Rodriguez, Relationship Between the Austenite Recrystallized Fraction and the softening Measured from the Interrupted Torsion Test Technique, *Scr. Mater.*, 1999, **40**(5), p 543–549 (in English)
15. C. Ouchi and T. Okita, Dynamic Recrystallization Behavior of Austenite in Nb-Bearing High Strength Low Alloy Steels and Stainless Steel, *Trans. ISIJ*, 1982, **22**, p 543–551 (in English)
16. "Metallography; Nondestructive Testing", ASTM Designation E112 in Annual Book of ASTM Standard, Part 3, V. 03.03, Philadelphia, PA, 1984, p 120
17. D.A. Porter and K.E. Easterling, *Phase Transformations in Metals and Alloys*, 2nd ed., Chapman & Hall, London, 1992 (in English)
18. K.J. Irvine, F.B. Pickering, and T. Gladman, Grain Refined C–Mn Steels, *J. Iron Steel Inst.*, 1967, **205**, p 161–182 (in English)
19. I. Weiss and J. Jonas, Interaction Between Recrystallization and Precipitation During the High Temperature Deformation of HSLA Steels, *Metall. Trans.*, 1979, **A10**(7), p 831–840 (in English)
20. S.F. Medina, Determination of Precipitation-Time-Temperature (PTT) Diagrams for Nb, Ti, or V Microalloyed Steels, *J. Mater. Sci.*, 1997, **32**, p 1487–1492 (in English)
21. S.F. Medina, The Influence of Niobium on the Static Recrystallization of Hot Deformed Austenite and on Strain Induced Precipitation Kinetics, *Scripta Metall. Mater.*, 1995, **32**(1), p 43–48 (in English)